Earth and Planetary Science Letters 581 (2022) 117410

Contents lists available at ScienceDirect

Earth and Planetary Science Letters

www.elsevier.com/locate/epsl

Major Early-Middle Devonian oceanic oxygenation linked to early land plant evolution detected using high-resolution U isotopes of marine limestones

Maya Elrick [a,*], Geoffrey J. Gilleaudeau [b], Stephen J. Romaniello [c], Thomas J. Algeo [d,e], Jennifer L. Morford [f], Monia Sabbatino [g], Tyler J. Goepfert [h], Christopher Cleal [i], Borja Cascales-Miñana [j], Pavel Chernyavskiy [k]

[a] Earth & Planetary Sciences, University of New Mexico, Albuquerque NM 87131, United States of America
[b] Department of Atmosphere, Oceanic & Earth Sciences, George Mason University, Fairfax VA 22030, United States of America
[c] Earth & Planetary Sciences, University of Tennessee, Knoxville, TN 37996, United States of America
[d] Geology Dept, University of Cincinnati, Cincinnati, OH 45221, United States of America
[e] State Key Labs of GPMR & BGEG, China University of Geosciences, Wuhan 430074, China
[f] Chemistry Dept, Franklin and Marshall College, Lancaster, PA 17604, United States of America
[g] Department of Mathematics and Geosciences, University of Trieste, Trieste, 34128, Italy
[h] School of Earth & Space Exploration, Arizona State University, Tempe, AZ 85287, United States of America
[i] Earth Sciences, University of Bristol, Bristol, BS8 1RL, United Kingdom
[j] CNRS, Univ. Lille, UMR 8198, Evo-Eco-Paleo, F-59000 Lille, France
[k] Department of Public Health Sciences, Division of Biostatistics, University of Virginia, Charlottesville, VA 22908, United States of America

ARTICLE INFO

Article history:
Received 19 November 2021
Received in revised form 22 January 2022
Accepted 29 January 2022
Available online xxxx
Editor: A. Jacobson

Keywords:
euxinia
seawater redox
middle Paleozoic
terrestrialization

ABSTRACT

The middle Paleozoic (~420-350 Myr) records a major increase in ocean-atmosphere oxygen levels; however, the timing and pattern of oxygenation are poorly constrained. Two well-dated North American locations in Nevada and Illinois were used to generate a high-resolution U-isotopic profile ($\delta^{238}U$) spanning ~70 Myr of the middle Paleozoic. Stratigraphic and geochemical data support the interpretation that the Nevada profile represents a near-primary record of global-ocean redox variations. First-order $\delta^{238}U$ trends indicate strongly reducing oceans during the late Silurian and Early Devonian, terminated by a major oxygenation event near the Emsian-Eifelian boundary (~395 Ma). More oxic seawater conditions persisted for the next 30+ Myr, but were punctuated by multiple Myr-scale anoxic events during the Middle-Late Devonian and Early Mississippian that correlate with known global biotic crises, positive $\delta^{13}C$ excursions, and widespread organic-rich facies deposition. The timing of the ~395 Ma oxygenation event suggests that the O_2 rise was the result of increased photosynthesis and organic carbon burial linked to diversification of late Silurian to earliest Middle Devonian terrestrial plants, rather than to subsequent Devonian increases in terrestrial plant root depth, tree height, lignin content, or seed reproduction. These findings demonstrate that early colonization of continents by relatively small, shallowly rooted plants with geographically limited ranges was sufficient to drive long-term oxygenation of the ocean-atmosphere system, paving the way for the evolution of large, mobile animals that have dominated the Earth's surface since the middle Paleozoic.

1. Introduction

The late Silurian-Devonian (middle Paleozoic; ~420-350 Myr) records a critical time in Earth history when continents were first colonized by vascular plants and vertebrates, atmospheric and oceanic O_2 rose and CO_2 levels generally declined, and the second of the 'Big Five' mass extinctions and smaller biotic crises occurred in conjunction with widespread marine anoxic events and biogeochemical cycle perturbations (Algeo and Scheckler, 1998; Dahl et al., 2010; Becker et al., 2016; Krause et al., 2018). Many of these environmental changes have been linked to the rise of early vascular land plants and plate tectonics (Algeo and Scheckler, 1998; Berner, 2006). The increase in atmospheric and oceanic O_2 is thought to have been due to a combination of increased produc-

* Corresponding author.
E-mail address: dolomite@unm.edu (M. Elrick).

https://doi.org/10.1016/j.epsl.2022.117410

tion and burial of refractory terrestrial and marine organic matter which decreased the sink for atmospheric O_2 (Berner, 2006). Devonian pCO_2 decreases are interpreted as the result of increased plant-induced silicate weathering and organic matter burial (Algeo and Scheckler, 1998; Berner, 1998), but see D'Antonio et al. (2020) for alternative interpretations. Devonian cooling in response to decreased pCO_2 led to significant glacio-eustatic changes, perturbations of the marine C-S-N cycles, and environmental stresses that contributed to mass extinctions and biotic crises (e.g., Chen et al., 2021b).

In this study we focus on the history of middle Paleozoic seawater oxygenation, building upon previous proxy and modeling studies that recognized a major oxygenation episode sometime in the ~60 Myr interval from the late Silurian to late Devonian (Scott and Glasspool, 2006; Algeo and Ingall, 2007; Sperling et al., 2015, 2021; Lenton et al., 2016; Wallace et al., 2017; Lu et al., 2018; Krause et al., 2018). This oxygenation event marked the shift to near-modern atmospheric pO_2, which is thought to have led to sustained ventilation of the deep oceans for perhaps the first time in Earth history and paved the way for large animal evolution in marine and terrestrial environments. The timing and pattern of this critical middle Paleozoic oxygenation rise are poorly constrained, however, because of the lack of a continuous global redox proxy record for the entire Devonian, low sample resolution in previous proxy and modeling studies, and disagreements on timing of the oxygenation shift. This temporal uncertainty hinders our ability to directly link rising O_2 levels with terrestrial plant diversification and organic carbon burial, thus leaving substantial ambiguity in our understanding of genetic linkages between these processes.

This study uses marine carbonate U isotopes and elemental geochemistry as a global seawater redox proxy to generate a ~70 Myr-long, high-resolution (biozone-level) record of Devonian seawater oxygenation and then compares that record to the most recent terrestrial plant diversity trends. The precise age control of our high-resolution seawater redox signal provides important new constraints on the linkages between terrestrial plant evolution and Paleozoic ocean-atmosphere redox, as well as a valuable baseline for a wide range of future Earth-system studies.

During the middle Paleozoic, Laurentia was located in the southern subtropics (Fig. S1). The Nevada study area in western Laurentia bordered the Panthalassic Ocean and accumulated 5-10 km of passive-margin and foreland basin deposits during the late Proterozoic through Early Mississippian. The Illinois intracratonic basin in eastern Laurentia contains up to 4.5 km of Paleozoic carbonates and siliciclastics, and during the Devonian was variably connected to the Rheic Ocean along a relatively narrow seaway (Kolata and Nelson, 1990; Fig. S1). Upper Silurian, Devonian, and Lower Mississippian carbonates from the study areas accumulated in a range of variably oxygenated, offshore through shoreface environments. Locations of studied sections, formations sampled, biostratigraphic age control and facies descriptions and interpretations are provided in Fig. S1 and Tables S1 and S2 and discussed in the Supplementary Materials (SM).

Uranium in nature is dominated by two long-lived isotopes, ^{238}U and ^{235}U, whose half-lives are 4.5 and 0.7 Gyr, respectively. The U isotope composition ($\delta^{238}U$, i.e., the permil deviation of the $^{238}U/^{235}U$ ratio relative to the CRM 145 standard) of seawater today is primarily controlled by the large isotopic fractionation associated with U removal to euxinic sediments/sinks, which underpins the utility of U isotopes as a paleo-redox proxy. Recent data also suggest that euxinia (not just general anoxia) is required to strongly fractionate U isotopes (Cole et al., 2020) and that there is a complex relationship between $\delta^{238}U$ values and areal extent of anoxic/euxinic sediments (Chen et al., 2021a). U is sourced to the oceans primarily via oxidative weathering of continental crust and river transport of dissolved U(VI). The average $\delta^{238}U$ value of major global rivers is −0.34‰, which is close to the isotopic composition of average continental crust (−0.31 ± 0.05‰; Tissot and Dauphas, 2015; Andersen et al., 2017). In seawater, U occurs in two oxidation states—relatively soluble U(VI) and particle-reactive, reduced U(IV). U(VI) forms stable, unreactive calcium-uranyl-bicarbonate complexes in seawater. Uranium has a residence time of ~400 kyr which is substantially longer than ocean mixing times (~1 kyr), resulting in a homogenous seawater U concentration and isotopic composition (−0.39 ± 0.01‰: Tissot and Dauphas, 2015).

The fractionation during U removal into euxinic sediments is driven by reduction of U(VI) to U(IV), which enriches the sediment in reduced $^{238}U(IV)$ and leaves seawater depleted in $^{238}U(VI)$. As a result, modern euxinic sediments record $\delta^{238}U$ values that are between 0.4‰ and 1.2‰ higher than seawater (Weyer et al., 2008). This fractionation factor is similar to that observed during microbially-mediated U(VI) reduction (−0.69 to −0.99‰; Stylo et al., 2015; Stirling et al., 2015). An increase in the global area of euxinic seafloor enhances removal of ^{238}U, thus driving the $\delta^{238}U$ composition of residual seawater towards lower values.

Chen et al. (2021a) reported that many Precambrian black shales (which should record the $\delta^{238}U$ value of the anoxic sink) have variable and lower $\delta^{238}U$ values than modern euxinic sediments. This same study also observed that Precambrian carbonates generally have $\delta^{238}U$ values near modern seawater despite a large body of evidence suggesting that the Precambrian oceans were largely anoxic (see also Gilleaudeau et al., 2019). These observations suggest either that: 1) low U residence times in the Precambrian oceans led to quantitative U removal and a lack of isotopic fractionation between seawater and both carbonates and black shales, or 2) U removal to Precambrian anoxic sediments was accompanied by a lower fractionation factor than is observed in modern euxinic settings. Cole et al. (2020) reported $\delta^{238}U$ data from modern and ancient ferruginous settings that revealed only a small degree of fractionation between water and ferruginous sediments and Bruggmann et al. (2022) report the same limited fractionation in modern low-oxygen, non-euxinic settings of the modern Peruvian upwelling zone. These data support the latter hypothesis and suggest that the largely ferruginous Precambrian oceans did not strongly fractionate U isotopes, which is the same conclusion drawn by Gilleaudeau et al. (2019). Ultimately, these data taken together suggest that U isotopes are useful for constraining the global extent specifically of euxinic seafloor, not just anoxic seafloor in general. Given that potentially low Precambrian U residence times are not likely to be an issue in the Devonian, we interpret our U isotope data as reflecting the global extent of ocean euxinia in the remainder of our discussion.

Several lines of evidence suggest that the $\delta^{238}U$ value of carbonate rocks can be used as a reliable proxy for ancient seawater U-isotope compositions. Calcite and aragonite precipitation experiments show only minor fractionation between dissolved and co-precipitated U (<0.13‰; Chen et al., 2018; Livermore et al., 2020), and measured $\delta^{238}U$ values of a variety of modern Bahamian abiotic and skeletal carbonates match that of seawater to within <0.1‰ (Romaniello et al., 2013). Holocene-Pleistocene Bahamian carbonates record $\delta^{238}U$ values that are up to 0.3‰ higher than seawater because of authigenic accumulation of U(IV) under sulfidic porewater conditions (Romaniello et al., 2013; Chen et al., 2018; Tissot et al., 2018). This holds regardless of carbonate mineralogy, depositional water depth, or core depth, suggesting that a uniform offset can be applied to carbonate data to reconstruct the approximate $\delta^{238}U$ composition of ancient seawater. del Rey et al. (2020) report that the carbonate matrix surrounding Silurian brachiopod shells (which presumably represent prevailing seawater values) can also be offset by up to 0.3‰, and that this offset depended on diagenetic fluid flow. Despite issues discussed above, the strongest evidence for the reliability of the carbonate $\delta^{238}U$

proxy as a global seawater redox proxy comes from comparing multiple, geographically widespread profiles spanning the Late Permian and Early Triassic that record nearly identical $\delta^{238}U$ trends of a ~0.5‰ negative shift (Brennecka et al., 2011; Lau et al., 2016; Elrick et al., 2017; Zhang et al., 2018).

2. Materials and methods

U isotope and elemental samples were collected at ~5-10 m (Nevada) and ~1 m (Illinois) intervals, chipped into small, non-weathered fragments, and powdered in a Spex shatterbox with an alumina puck pulverizer. Powders were dissolved in 1 M HNO_3 and solutions were centrifuged to remove insoluble residues. A 1 M HNO_3 dissolution has been used in a number of recent studies (e.g., Gilleaudeau et al., 2019) and Clarkson et al. (2020) also document that a variety of dissolution methods produce indistinguishable U isotope results. A solution split was diluted to ~200 ppm Ca with 2% HNO_3 and analyzed for a full suite of major, trace, and rare-earth element abundances on a Thermo Scientific ICAP-Q inductively coupled plasma mass spectrometer (ICP-MS) at Arizona State University. The analytical precision for all elements of interest was <5%. The remaining solution was dried down, spiked with an appropriate amount of IRMM $^{233}U/^{236}U$ double-spike (0.8 mL of spike per 500 ng U), and digested using reverse aqua regia, H_2O_2, and concentrated HNO_3, with the sample eventually dissolved in 3 M HNO_3 before column chemistry. U was then separated from matrix elements by ion exchange chromatography using UTEVA resin. Purified U was dissolved in 2% HNO_3 to a concentration of ~50 ppb and analyzed on a Thermo Scientific Neptune multi-collector ICP-MS at ASU. The long-term accuracy and reproducibility of $\delta^{238}U$ values in the ASU laboratory is better than 0.07‰ (2 s.d.) based on routine analysis of primary and secondary isotopic standards, long-term reproducibility of standard reference materials (BCR-2, SDO-1), and inter-laboratory comparison exercises (Andersen et al., 2017; Elrick et al., 2017). Analytical mass spectrometry precision is reported here as 2 s.d. of replicate measurements for each sample, with most samples measured at least three times. Further details on the analytical methods can be found in Brennecka et al. (2011).

Samples for C-O stable isotope analysis were collected at ~1-5 m intervals and samples were processed as reported in Spotl and Vennemann (2003) at the University of New Mexico Center for Stable Isotopes. The results are reported using the delta notation versus V-PDB. Reproducibility was better than 0.1‰ for both $\delta^{13}C$ and $\delta^{18}O$ based on repeated analysis of a laboratory standard (Carrara Marble). The laboratory standards were calibrated versus NBS 19 ($\delta^{13}C = +1.95$‰ and $\delta^{18}O = -2.20$‰).

The cerium anomaly (Ce/Ce*) has been calculated using rare earth elemental data using the following equation: $Ce/Ce^* = [Ce]_{SN}/([Pr]_{SN}^2/[Nd]_{SN})$, with SN referring to shale-normalized values where the concentration of these elements in the sample is divided by the concentration in Post-Archean Australian Shale (PAAS; Taylor and McLennan, 1985). Using the same shale normalizations, the europium anomaly (Eu/Eu*) has been calculated using the following equation: $Eu/Eu^* = (2^*[Eu]_{SN})/([Sm]_{SN} + [Gd]_{SN})$.

3. Results

3.1. $\delta^{238}U$, $\delta^{13}C$, $\delta^{18}O$ trends

Nevada $\delta^{238}U$ values are low (~−0.6‰) through much of the upper Silurian-Lower Devonian with a brief positive shift near the Lochkovian-Pragian boundary (Fig. 1). Values decrease systematically in the Pragian, are relatively stable and lower during the Emsian, and abruptly increase by ~0.4‰ across the Emsian-Eifelian unconformity. Values then remain high (~−0.35‰) for the remainder of the Devonian and into the Lower Mississippian. Seven Myr-scale negative excursions are superimposed on the higher post-Emsian isotopic values. $\delta^{13}C$ profiles are characterized by large Lower Devonian excursions, more stable upper Lower and Middle Devonian values, followed by large positive excursions in the Upper Devonian and Lower Mississippian (Fig. 1, Table S4). The $\delta^{18}O$ profile is characterized by a large negative Lochkovian excursion with predominantly low values and wide scatter (−15.0‰ to −3.0‰), a distinct shift to higher and more invariant values (~-3.0‰) into the lower Frasnian, followed by an abrupt shift to lower values (~-8.0‰) in the remainder of the Upper Devonian (Fig. S3).

3.2. Elemental trends

Stratigraphic trends and crossplots of selected trace and rare-earth elements (REE), weight percent carbonate (wt.% carb), and U enrichment factor (U_{EF}) of samples from Nevada and Illinois are shown in Figs. S4, S5, and S6 and Table S1; we focus here on reporting the Nevada results. Mn/Sr values are <1 except for five samples, and no covariation between $\delta^{238}U$ and Mn/Sr is observed. U concentrations range from 0.1 ppm to 3.17 ppm (median = 0.42 ppm); these values lie within the range of typical Paleozoic limestones, whereas typical modern/Pleistocene aragonite concentrations are ~2-4 ppm (Romaniello et al., 2013; Chen et al., 2018). Wt.% carb ranges are from 55 to 96% (median = 84%) with the lowest values in the Lochkovian; crossplots against $\delta^{238}U$ show no covariation. Average U_{EF} values are 132 with the highest values in the mid-Lochkovian and across the Emsian-Eifelian boundary. Mg/Ca ratios range from <0.1 to 1.2 (median = 0.2) with four samples (field-identified dolomites) recording values >0.5. Ce/Ce* values are universally <1 with the consistently highest values (but still <1) in the Lochkovian and briefly in the mid and upper Eifelian and upper Givetian. Eu/Eu* values are close to 1 for all but the upper Lochkovian and near the Silurian-Devonian boundary.

4. Discussion

4.1. Evaluating local depositional and diagenetic influences

4.1.1. Stratigraphic evidence

In contrast to $\delta^{238}U$ studies in siliciclastic mudrock/shales where the U-isotope signal is derived from detrital grains, diagenetic U(VI) reduction in the sediments, and/or post-depositional authigenic sources, $\delta^{238}U$ values from limestones record U incorporated into carbonate minerals as they precipitate from seawater and/or porewaters. Phanerozoic limestones are composed of a combination of minerals precipitated by carbonate-secreting organisms and microbial communities (both living in the photic zone), as well as finer grained detrital/abraded carbonate material and diagenetic cements. These origins indicate that even though the skeletal material and detrital carbonate particles may have accumulated in poorly- to well-oxygenated deeper-water settings, the authigenic U component (minus any diagenetic cements) reflects shallow-water or photic zone conditions that may not match *in situ* depositional redox interpretations.

Comparisons between depositional redox conditions for the Nevada facies and $\delta^{238}U$ values show no relationship (Figs. 1, S3). For example, Emsian offshore facies, interpreted to have been deposited in poorly oxygenated settings based on field observations, would be expected to have the highest $\delta^{238}U$ values due to limited bottom-water circulation and oxygen concentrations leading to enhanced porewater anoxia and precipitation of carbonate cements enriched in isotopically heavy U. Instead, these facies record some of the lowest $\delta^{238}U$ values. Conversely, well-oxygenated grainstone facies deposited in high-energy, shoreface environments and with

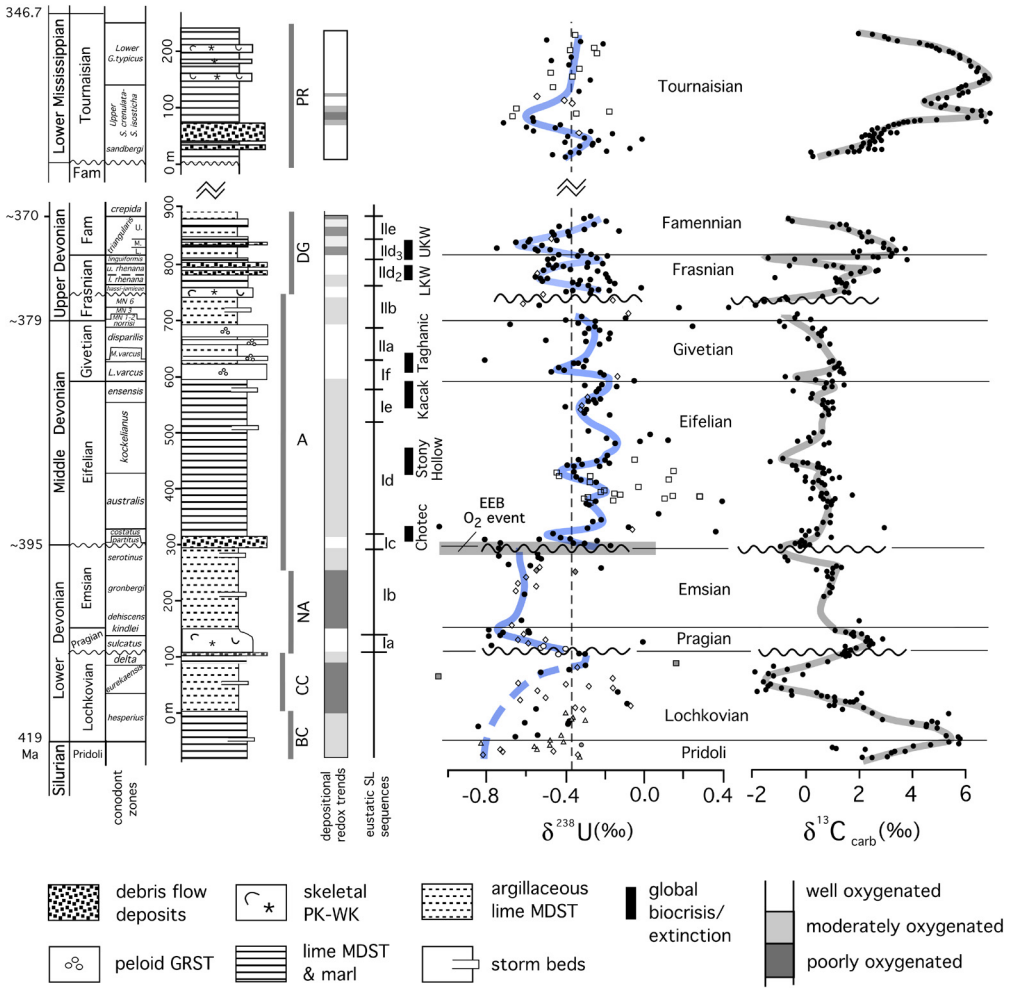

Fig. 1. Stratigraphic, depositional redox, eustatic depositional sequences, $\delta^{238}U$, and $\delta^{13}C$ from the Nevada section. Six stratigraphically contiguous sections include BC = Birch Creek, CC = Coal Canyon, NA = northern Antelopes, A = northern Antelopes, DG = Devil's Gate, and PR = Pahranaghat Range (see Table S1) were used to generate the composite Nevada record. Facies descriptions, age control, and section information are reported in Tables S1, S2 and SM. Eustatic sea-level cycles (TR cycles) are from Johnson et al. (1996). Blue $\delta^{238}U$ curve is best fit using lowest $\delta^{238}U$ values, which are assumed to be least altered as discussed in the text; curve smoothing using algorithms of Schneider (1990). Dashed portion of $\delta^{238}U$ blue curve identifies least confident interval due to post-depositional alteration as discussed in text. EEB O_2 event = Emsian-Eifelian boundary oxygenation event. Labeled black vertical lines outline global biocrises/extinctions that correlate to Myr-scale negative $\delta^{238}U$ excursions and are taken from Becker et al. (2016). LKW = lower Kellwasser extinction, UKW = upper Kellwasser extinction. Dashed vertical line shows modern seawater $\delta^{238}U$ values. Symbols used in $\delta^{238}U$ curve indicate data points with geochemical values lying outside conventional ranges interpreted as 'altered' and include: open triangle = Y/Ho < 40, open diamond = wt.% carb < 80, open square = U_{EF} < 50, shaded square = wt.% carb < 80 and Y/Ho < 40, shaded diamond = wt.% carb < 80 and U_{EF} < 50, shaded triangle = U_{EF} < 50 and Y/Ho < 40, shaded circle = U_{EF} < 50 and Mn/Sr > 5, open circles = dolomite, black circles = all data points with values lying within conventional ranges defined as 'least altered'. Time scale from Becker et al. (2020). Most Frasnian and Famennian data from White et al. (2018); GRST = grainstone, PK = packstone, WK = wackestone, MDST = lime mudstone; Early Mississippian data from Cheng et al. (2020). (For interpretation of the colors in the figure(s), the reader is referred to the web version of this article.)

significant early marine cements (implying active porewater circulation and communication with the overlying oxygenated water column), should exhibit minimal effects of porewater anoxia and the least ^{238}U enrichment. Instead, these facies record relatively higher $\delta^{238}U$ values. The lack of facies control on $\delta^{238}U$ values is also suggested by the range and median of $\delta^{238}U$ values, which overlap for well-oxygenated and poorly-oxygenated facies (Fig. S5C).

Additional stratigraphic observations also argue against local redox controls, facies-related diagenesis, or Myr-scale eustatic fluctuations influencing $\delta^{238}U$ trends. First, samples collected from shoreface grainstone layers intimately interbedded with offshore lime mudstone layers record the same $\delta^{238}U$ values (Fig. S3). Myr-scale $\delta^{238}U$ shifts observed throughout the studied interval are recorded across stratigraphic intervals with no facies changes, as well as across intervals composed of the full range of facies (Fig. S3). Finally, no systematic $\delta^{238}U$ shifts are observed across 11 of the 12 Devonian sequence boundaries generated by eustatic sea-level rise/falls (Fig. 1). Combined, these relationships argue against local processes exerting significant control on observed $\delta^{238}U$ trends in the Nevada section.

4.1.2. Diagenetic and detrital indicators

The majority of samples yielded Mn/Sr values less than 1, indicating little influence by diagenesis, which is confirmed by the lack of covariation of Mn/Sr with $\delta^{238}U$ (Figs. S4, S6). Median Mg/Ca values of 0.2 indicate that dolomitization did not influence $\delta^{238}U$ values (Fig. S6). Stratigraphic trends of wt.% carb do not covary with depositional redox trends, nor do crossplots of wt.% carb against $\delta^{238}U$ (Figs. S4, S6). U_{EF} trends indicate that all samples are highly enriched in U relative to average crustal values, suggesting a large authigenic U component in the study samples (McLennan, 2001; Fig. S4). The upper Lochkovian Eu anomaly (section CC) suggests possible hydrothermal fluid influences related to Cenozoic dike intrusions observed throughout the study area.

4.1.3. Local geochemical redox indicators

All samples have Ce/Ce* values <1 with the lowest values (<0.5; most oxic; see SM discussion) in the upper Lochkovian through lower Eifelian and briefly in the mid-Eifelian, Givetian, and lower Frasnian. These trends are consistent with the interpretation that the Nevada samples record predominantly oxic watermass conditions with the least oxic conditions in the Lochkovian and briefly in the Middle Devonian (Wallace et al., 2017). Ce/Ce* against $\delta^{238}U$ shows no covariation, indicating that local redox conditions did not strongly influence the $\delta^{238}U$ signal (Fig. S6). I/Ca ratios for a portion of the Nevada composite section are reported by He et al. (2021).

4.2. C-O stable isotopes

Comparison with coeval $\delta^{13}C$ records worldwide (van Geldern et al., 2006; Buggisch and Joachimski, 2006; Saltzman et al., 2012; Becker et al., 2020) shows that the Nevada $\delta^{13}C$ record represents a robust global signal (Fig. 1). First-order (10^7 yr) temporal relationships between $\delta^{13}C$ and $\delta^{238}U$ trends are inversely correlated with the lowest $\delta^{13}C$ values in the Middle Devonian associated with the highest baseline $\delta^{238}U$ values at the same time (Fig. 1). This relationship adds support to the interpretation that the Nevada $\delta^{238}U$ record reflects near-primary seawater redox conditions and suggests that the intervals with lower $\delta^{13}C$ values are best explained by more oxic global oceans limiting widespread organic carbon preservation and burial. Second-order (10^6 yr) $\delta^{13}C$ vs $\delta^{238}U$ relationships are also dominantly inversely correlated with minor intervals of positive covariation. Negative covariations have been noted in previous $\delta^{238}U$ studies with temporal offsets between $\delta^{238}U$ and $\delta^{13}C$ excursions, likely because increased organic carbon burial is not always tightly linked to expanded seawater anoxia (Dahl et al., 2014; Song et al., 2017; Cheng et al., 2020).

Deep-time $\delta^{18}O_{carb}$ records are notoriously prone to diagenetic alteration. The low and widely scattered $\delta^{18}O$ values during the Lochkovian (Fig. S3) likely reflect alteration by burial fluids with elevated temperatures, and an interpretation of post-depositional hydrothermal influences in these samples is supported by elevated Eu/Eu* values. Despite this, the overall negative $\delta^{18}O$ excursion in the upper Lochkovian-Pragian is similar to trends in coeval $\delta^{18}O_{apatite}$ records that are more resistant to diagenetic alteration (Joachimski et al., 2009). We acknowledge that the $\delta^{18}O_{carb}$ profile shows evidence for diagenetic alteration in this specific part of the section, but note that alteration is known primarily to increase $\delta^{238}U$ values, therefore we use the minimum $\delta^{238}U$ values to assess Lochkovian seawater redox. Pragian through mid-Frasnian $\delta^{18}O$ values are relatively high (>−5‰) and have limited scatter (excluding the mid-Eifelian) and are in general agreement with the global $\delta^{18}O_{apatite}$ record (Becker et al., 2020). The combined $\delta^{18}O$ and $\delta^{13}C$ trends provide compelling evidence that the Nevada $\delta^{238}U$ curve represents a near-primary seawater redox record. The two intervals of substantially lower $\delta^{18}O$ values (Lochkovian and mid-Eifelian) are also characterized by wide $\delta^{238}U$ scatter, suggesting some degree of alteration during these specific intervals and we interpret values from these intervals with caution. However, the majority of the Nevada $\delta^{238}U$ record outside of these discrete intervals appears to be well-preserved.

4.3. Laurentian-wide $\delta^{238}U$ comparisons

Comparisons between the Nevada and Illinois sections are made at the stage and conodont zone level; consequently, the position of individual data points or shifts *within* individual zones/stages cannot be evaluated (Fig. 3). For example, the apparent opposing trends in the *hemiansatus* Zone could be the result of incomplete sampling of the full zone in either section or due to variable sedimentation rates at one or both sites. The Nevada and Illinois profiles record clear overlap in absolute $\delta^{238}U$ values and trends in the early *serotinus, costatus*, and *australis* zones, and values overlap in the *kockelianus* and *hemiansatus* zones. Within the Pragian, lower Emsian, and upper Emsian, the Illinois $\delta^{238}U$ profile shows similar trends to the Nevada profile, but is consistently enriched by ~0.2-0.4‰ (Fig. 3). The higher Illinois $\delta^{238}U$ values coincided with an interval during which the Illinois Basin was more isolated from the Rheic Ocean due to low global sea level (Fig. S1). As a result, the influence of river systems entering the Illinois Basin on watermass $\delta^{238}U$ was greater during that interval. The high detrital quartz sand content in the Lower Devonian Illinois samples (Table S1) support the interpretation of increased fluvial input. Long-term global sea-levels rose subsequently through the Eifelian-Frasnian (Johnson et al., 1985) presumably expanding the connection to the Rheic Ocean and backstepping fluvial systems. Recent studies making use of elemental salinity proxies and related data have demonstrated brackish conditions and a pronounced salinity gradient in the Illinois and Appalachian basins during the Late Devonian (Song et al., 2021; Gilleaudeau et al., 2021). In fact, recent work on cratonic-interior seaways from multiple continents and from a range of ages has shown that many of seaways experienced brackish rather than fully marine conditions, demonstrating that the long-held assumption of marine conditions in such basins requires re-evaluation.

The position of the Nevada section on the western Laurentian margin adjacent to the Panthalassic Ocean largely obviates such local influences, suggesting that the Nevada section is more likely to have recorded primary global-ocean $\delta^{238}U$ values during the Pragian and Emsian, as well as later. Exclusive of the Lower Devonian, the similarities in $\delta^{238}U$ values and trends between two study sections that were separated by >2800 km across Laurentia support our interpretation that the Nevada $\delta^{238}U$ profile represents a near-primary global marine signal.

4.4. Seawater redox trends

Typical carbonate sediment diagenesis, hydrothermal alteration, and local depositional influences (freshwater influx, terrestrial sediment contamination) are known to enrich primary marine $\delta^{238}U$ values (Chen et al., 2018; Tissot et al., 2018). Given this, we use the lowest (least-altered) values to generate the best-fit curve shown in Fig. 1. To verify the first-order $\delta^{238}U$ trends, we analyzed the Nevada dataset using a range of statistical tests discussed in the SM.

$\delta^{238}U$ values for the upper Silurian (Pridoli) and Lochkovian record the effects of variable post-depositional alteration; however, their overall pattern using either the lowest values or successive conodont zone-level average values offers evidence of initially low Pridoli $\delta^{238}U$ values that increased into the Lochkovian (Fig. 1). This pattern is consistent with a shift from more reducing oceans in the late Silurian to more oxic seawaters near the Lochkovian-Pragian boundary. Subsequently, a ~0.4‰ negative $\delta^{238}U$ shift occurred over <2 Myr during the Pragian, indicating a return to more reducing seawater conditions that continued through the Emsian.

Other studies have similarly suggested overall reducing oceans during the mid to late Silurian using U and Tl isotopes, $\delta^{34}S$, I/Ca, Fe-speciation, trace metal concentrations, frequency of large positive $\delta^{13}C$ excursions associated with biotic turnovers, and the abundance of organic-rich facies (Calner, 2008; Young et al., 2019; Bowman et al., 2019, 2020; Cole et al., 2020; Melchin et al., 2020; del Rey, 2021; Sperling et al., 2021). Combined with our predominantly low $\delta^{238}U$ values from the upper Silurian-Lower Devonian, these data record a ~20-Myr interval spanning the mid-late Sil-

urian to Early Devonian during which the global ocean was significantly more reducing than today.

$\delta^{238}U$ values record a major positive shift of >0.4‰ across the unconformable Lower-Middle Devonian boundary (Emsian-Eifelian boundary or EEB, ~395 Ma). The apparent abruptness of this shift is a result of a <4 Myr hiatus along the unconformity. We estimated the hiatal duration based on the number of missing conodont zones, which includes the Emsian late *serotinus* and *patulus* zones (~3 Myr) and much of the Eifelian *partitus* zone (~1 Myr; Becker et al., 2020). When considering the interpretation of this positive $\delta^{238}U$ shift, we considered the range of redox-sensitive processes that can affect global seawater $\delta^{238}U$ values. Whereas euxinic sinks are well-constrained to strongly fractionate U isotopes by incorporating ^{238}U into sediments (leaving residual seawater enriched in ^{235}U), U-isotope fractionation associated with less reducing sinks such as ferruginous and suboxic sediments is more poorly constrained. Cole et al. (2020) presented data from a variety of modern and ancient ferruginous environments that suggested muted fractionation during U removal to sediments under ferruginous conditions, implying that strong fractionation is specifically linked to euxinia. Thus, a shift towards higher seawater $\delta^{238}U$ values can be interpreted as a shift towards more oxygenated oceans or as a shift in the primary redox buffer of anoxic oceans away from H_2S (euxinic conditions) and towards Fe(II) (ferruginous conditions). This is an important distinction because Gilleaudeau et al. (2019) reported relatively high $\delta^{238}U$ values (~−0.4‰) across a variety of mid-Proterozoic carbonates that were deposited in a generally low-O_2 ocean-atmosphere system, suggesting that this isotopically-heavy signal represents largely ferruginous rather than more oxic oceans.

We consider it more likely that the prominent EEB positive $\delta^{238}U$ shift represents a true oxygenation event, rather than a shift to a more ferruginous ocean. This is because of a fundamental difference in the redox balance of mid-Proterozoic oceans compared to their later Phanerozoic counterparts. During the mid-Proterozoic, a persistently anoxic deep ocean was likely maintained by atmospheric pO_2 much lower than today (perhaps as low as 1-4% of the present atmospheric level; Planavsky et al., 2014; Zhang et al., 2016). Euxinia was not a major feature of these low-O_2 oceans (Planavsky et al., 2014; Gilleaudeau et al., 2019), however, likely because of both low seawater sulfate concentrations (Kah et al., 2004) and low primary productivity rates related to general phosphorous-limitation (Laakso and Schrag, 2014), as both sulfate and organic carbon are required to fuel microbial sulfate reduction. Instead, Fe(II) from hydrothermal sources dominated the deep anoxic oceans of the mid-Proterozoic (Clarkson et al., 2018). In contrast, higher atmospheric pO_2 and oceanic sulfate concentrations beginning sometime in the early Paleozoic, as well as generally higher primary productivity rates compared to the mid-Proterozoic, would likely have favored euxinia over ferruginous anoxia beginning at least by the Devonian. Sperling et al. (2021) presented a long-term Fe-speciation record through the early and middle Paleozoic that revealed a shift from predominantly ferruginous conditions in the early Paleozoic to the development of local euxinia by the Early Devonian. They interpreted these results as due to increased primary productivity/export production linked to plant-weathering feedbacks (see below). In summary, euxinia became the dominant type of ocean anoxia at least by the Devonian (and continuing to today), therefore it is unlikely that the positive $\delta^{238}U$ shift at the EEB recorded in this study represents a shift back to Proterozoic-style ferruginous oceans.

After the positive $\delta^{238}U$ shift at the EEB, baseline $\delta^{238}U$ values remained relatively high (average = ~−0.35‰) throughout the rest of the Devonian and into the Lower Mississippian, suggesting that more oxygenated oceans persisted for >30 Myr after the ~395 Ma event. Three-sink mass balance modeling (Gilleaudeau et al., 2019) suggests that a seawater $\delta^{238}U$ value of −0.3‰ corresponds to a maximum euxinic seafloor area of only 0.1%. Even with the application of a positive 0.3‰ diagenetic offset (i.e., Chen et al., 2018) to Middle-Upper Devonian measured carbonate $\delta^{238}U$ values of ~-0.3‰, yields estimates of Devonian seawater $\delta^{238}U$ values as low as −0.6‰ and a modeled maximum euxinic seafloor area of only 1.5%. This model is scaled to reflect U burial rates in oxic, anoxic and non-euxinic, and euxinic environments, and is aimed at quantifying redox conditions across the global seafloor (Gilleaudeau et al., 2019). It is difficult to estimate the extent of other anoxic sinks (such as ferruginous sediments) on the global seafloor because of smaller and uncertain fractionation factors during U removal under ferruginous conditions (Cole et al., 2020). Regardless, the positive $\delta^{238}U$ shift indicates a substantial decrease in seafloor euxinia, which is interpreted as recording a major oceanic oxygenation event at ~395 Ma.

Previous $\delta^{238}U$ studies of the late Paleozoic (e.g., Zhang et al., 2018), Mesozoic (Jost et al., 2017; Clarkson et al., 2018; Herrmann et al., 2018), and Cenozoic (Wang et al., 2016) indicate that near-modern to modern oceanic oxygen levels persisted from the Middle Devonian onward with the exception of discrete anoxic events that were often associated with mass extinctions and biogeochemical cycle perturbations. This highlights the significance of the EEB oxygenation rise in the context of Phanerozoic seawater redox history (Fig. 2). A major late Silurian-Devonian oxygenation event was documented in previous studies using independent redox proxies, including Mo isotopes and concentrations (Dahl et al., 2010), Fe-speciation (Sperling et al., 2015, 2021), I/Ca ratios (Lu et al., 2018), C_{org}:P ratios in organic-rich facies (Algeo and Ingall, 2007), charcoal abundance (Scott and Glasspool, 2006), Ce/Ce* in marine carbonates (Wallace et al., 2017), and modeling data (Lenton et al., 2016; Krause et al., 2018). However, due to the low sample resolution of most of the previous redox studies, the timing of the shift was only broadly constrained to the late Silurian to Late Devonian interval—a time span of ~60 Myr. Our near-continuous and high-resolution $\delta^{238}U$ record, which permits biozone-level age control, constrains the timing and duration of the oxygenation event as spanning <4 Myr beginning sometime within the latest Emsian (late *serotinus* and *patulus* zones) to the earliest Eifelian (early-mid *partitus* Zone).

The overall more oxic seawater conditions of the ensuing Middle-Late Devonian and Early Mississippian interval were punctuated by at least seven, high-frequency (Myr-scale) $\delta^{238}U$ negative excursions recording brief anoxic events (Fig. 1). The early Eifelian (*costatus* Zone) negative excursion was coeval with the globally recognized Choteč biotic crisis and anoxic event (Chlupáč and Kukal, 1986). The mid- and late Eifelian negative excursions were coeval with the Stony Hollow (*kockelianus* Zone) and Kačak (*ensensis* Zone) biotic crises, respectively, and the early Givetian (L.-M. *varcus* Zone) excursion may have coincided with the Taghanic biotic crisis, all of which were associated with global deposition of anoxic facies (Becker et al., 2016). Previous studies documented the relationships between the Late Devonian mass extinction event (upper and lower Kellwasser), negative $\delta^{238}U$ excursions, and widespread anoxic facies deposition (Song et al., 2017; White et al., 2018). The recognition of these linkages between anoxia and biotic crises emphasizes the importance of developing continuous and high-resolution seawater redox records for the entire Phanerozoic, and we acknowledge that further high-resolution paired U- vs C-isotope studies are warranted on the Middle Devonian interval.

4.5. Terrestrial plant evolution and seawater redox relationships

We investigated potential linkages between seawater redox changes and terrestrial plant evolution by comparing our global seawater $\delta^{238}U$ curve with evolutionary changes in middle Pa-

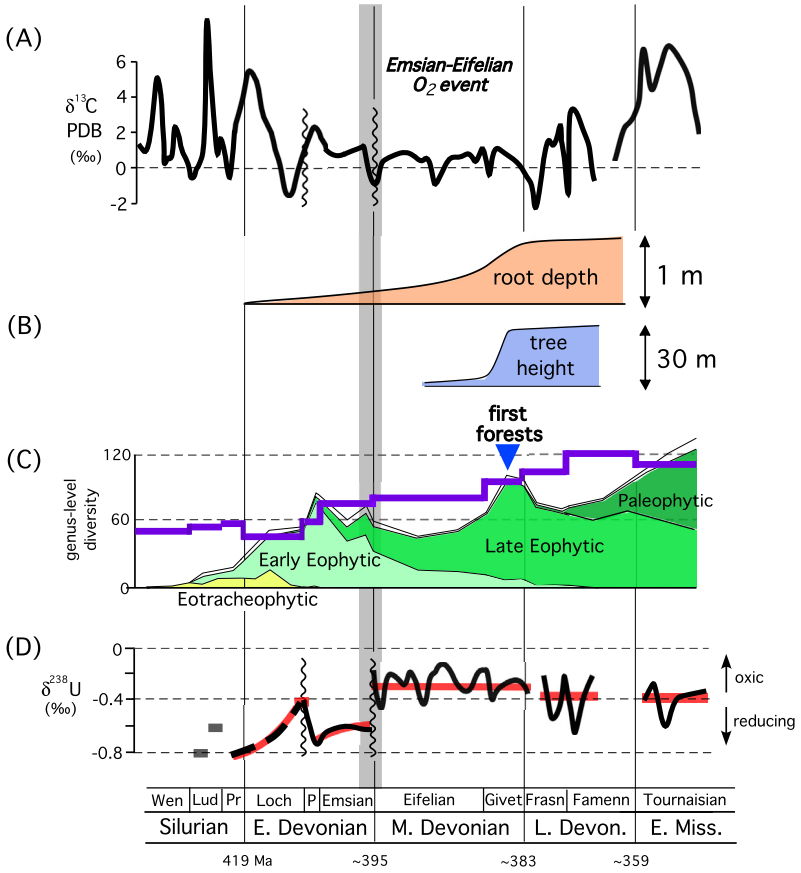

Fig. 2. Middle Paleozoic global seawater $\delta^{238}U$, terrestrial plant evolutionary, and $\delta^{13}C$ trends. A) The late Silurian through Devonian-Early Mississippian $\delta^{13}C$ curve is from this study and the middle-late Silurian $\delta^{13}C$ curve is from Saltzman et al. (2012). B) Changes in root depths, tree heights, and the onset of first forests (blue triangle) from Algeo and Scheckler (1998). C) Genus-level terrestrial plant diversity trends; purple curve represents spore diversity from Cascales-Miñana (2016), green and yellow shading outlines vascular plant diversity trends and Evolutionary Flora (discussed in text) are from Capel et al. (2021). D) $\delta^{238}U$ trends from this study, black curve is best fit line shown in Fig. 1, red lines approximate average isotopic trends over specific time intervals. Additional dark gray late Silurian $\delta^{238}U$ data are from previous $\delta^{238}U$ studies (Cole et al., 2020; del Rey et al., 2020). Gray shaded vertical band outlines the major Emsian-Eifelian seawater oxygenation event identified in this study. Wen = Wenlock, Lud = Ludlow, Pr = Pridoli, Loch = Lochkovian, P = Pragian, Givet = Givetian, Frasn = Frasnian, Famenn = Famennian, E. = Early, M. = Middle, L.= Late.

leozoic terrestrial vegetation (Fig. 2). The genus-level land plant diversity record shown in Fig. 2 indicates a progressive increase in taxonomic richness through the studied time interval. However, such diversity curves based on the macrofloral record can be influenced by inherent taphonomic and rock record biases (Smith and McGowan, 2007; Kenrick et al., 2012; Cascales-Miñana et al., 2013; Cleal and Cascales-Miñana, 2021). In this case, the observed diversification may in part reflect the increased prevalence of terrestrial deposits (versus marine deposits) that would favor the preservation of plant macrofossils. The palynological (spore) record is potentially less biased because spores are found in both marine and terrestrial deposits and they are highly resistant to post-depositional alteration processes (Wellman et al., 2013). However, palynological diversity does not reflect plant diversity because the relationship between spores and many pre-Carboniferous plants known from macrofossils is incompletely understood. Because of these inherent biases in the macrofloral record, we focus on the *timing* of major plant evolutionary changes rather than primarily on quantitative taxonomic diversity trends in our comparisons to the seawater redox curve.

We interpret the global history of vegetation from the Silurian through Mississippian using the Evolutionary Floras model of Cleal and Cascales-Miñana (2021). Like the Evolutionary Faunas model of Sepkoski (1984), the Evolutionary Floras model was based on a factor analysis of a family-rank dataset. It reveals a succession of five discrete floras through the Phanerozoic, each characterized by a group of coexisting plant families and orders that formed relatively coherent communities in time and space. This is supplemented by a similar analysis of a genus-rank dataset for Devonian floras (Capel et al., 2021). The combined paleobotanical model resolves the Silurian to Mississippian plant fossil record into Eotracheophytic, Early and Late Eophytic, and Paleophytic floras, with the transition between successive floras being marked by the appearance of major evolutionary adaptive innovations.

The Eotracheophytic flora represented the transition from subaquatic to subaerial vegetation. There is palynological and some macrofloral evidence of terrestrial vegetation from the Ordovician (Servais et al., 2019), and molecular clock estimates suggest a possible Cambrian origin (Kenrick et al., 2012), but the oldest unequivocal macrofossil evidence of eutracheophytes is from the middle Silurian. The Eotracheophytic flora was dominated by basal eutracheophytes and rhyniophytoids, and known macrofossils are slender, leafless stems with terminal sporangia. There is little preserved evidence of the lower parts of these plants and it is possible that the fossils were reproductive structures of partly subaquatic plants that were exposed to facilitate the dispersal of the spores (Servais et al., 2019). They nevertheless represent the initial steps in the terrestrialization process and in diversification of vascular plants during the Ordovician to earliest Devonian (Capel et al., 2021).

Eotracheophytic plant size was constrained by their stem structure, with support for subaerial growth being mainly limited to turgor in the cortical tissue and sometimes an outer zone of thickened cells (Edwards et al., 1986). Consequently, eutracheophytes

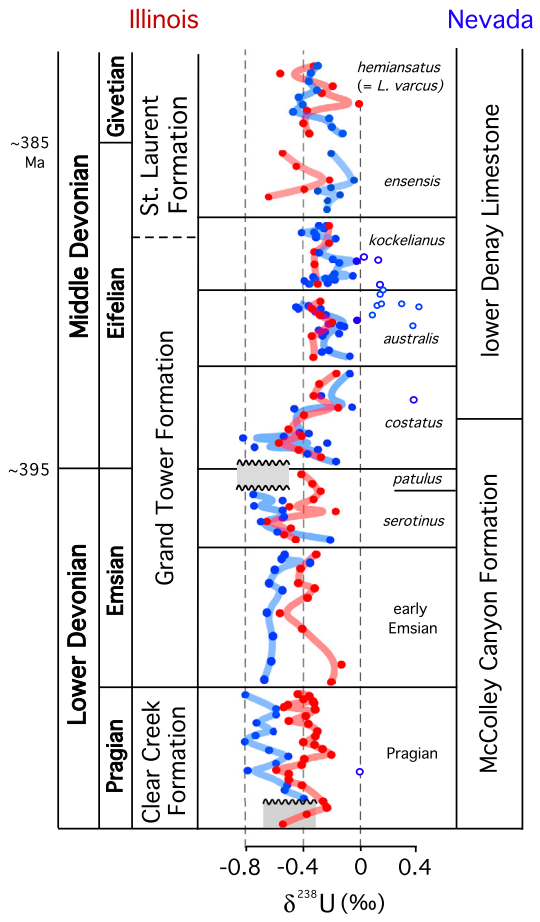

Fig. 3. Coeval Nevada (blue) and Illinois (red) $\delta^{238}U$ trends. Gray shaded region marks hiatuses along Nevada unconformities. Open circles are identified as significantly enriched in ^{238}U during diagenesis. See text for detailed discussion of comparisons.

were no more than 2 cm tall (usually less) and so represented very little biomass. The rooting structures, if any, had few effects on substrate conditions. Given this, there is little evidence that this early flora had much impact on oceanic redox trends and $\delta^{238}U$ values remained predominantly low, indicating relatively reducing seawater conditions.

Plants underwent a fundamental change in the late Silurian and especially the Early Devonian with the appearance of the Early Eophytic flora. This is when the first unequivocal examples of fully terrestrial plants with true rhizomorphic stems and rooting structures appeared (Hetherington et al., 2021). They were much taller than the Eotracheophytic plants as the stems had developed a thicker vascular system for transporting water and nutrients and much-improved mechanical support for upright growth. The Early Eophytic taxa, which were dominated by zosterophyllopsids, trimerophytopsids, and early lycopsids, grew to perhaps 0.5 m in height.

The Early Eophytic flora shows a major peak in taxonomic diversity during the late Pragian (Fig. 2). However, although more than an order of magnitude taller than Eotracheophytic plants, the Early Eophytic flora was still relatively small, and their photosynthetic structures were limited to spines and small microphylls (small, single-veined leaves). It seems unlikely, therefore, that this vegetation would have significantly influenced overall levels of photosynthesis and biomass burial. Although a large upper Lochkovian positive $\delta^{238}U$ shift in our dataset suggests more oxic seawater conditions, it seems unlikely that this was caused by a diversifying Early Eophytic flora.

The next major change was the appearance of the Late Eophytic flora, dominated by cladoxylopsids, rhacophytopsids, subarborescent lycopsids, and early progymnosperms. These plants developed more complex stem anatomies and larger leaves (Meyer-Berthaud et al., 2010), allowing them to grow much larger and to form incipient forest-like ecosystems. After peaking in the Pragian, the taxonomic diversity of the Early Eophytic flora declined significantly during the Emsian, and the Late Eophytic flora did not diversify significantly until the Eifelian (Fig. 2). This Eifelian diversification would have had a significant impact on terrestrial systems in that it facilitated vegetation spread into a much wider range of habitats, and these larger plants were more deeply rooted and had a much greater biomass than the preceding Early Eophytic flora.

The explosive diversification of the Late Eophytic flora in the Eifelian coincided with the onset of more positive $\delta^{238}U$ values in our seawater redox record, indicating a shift to more oxygenated seawater conditions. The development of incipient forest-like ecosystems with much larger plants and leaves implies significantly increased levels of terrestrial photosynthesis and biomass burial, raising atmosphere and oceans oxygen levels. However, this change did not coincide with an increase in taxonomic diversity but, rather, with a fundamental change in plant bauplans (structural plans) and anatomies. In the Givetian, there was rising taxonomic diversity, the appearance of the first true forests and increases in tree heights, lignin content, and root depths—probably as a consequence of the structural changes (Algeo and Scheckler, 1998). Interestingly, these innovations did not apparently alter long-term seawater oxygen levels.

Vegetation underwent a major change in the Late Devonian with the rapid diversification of the Paleophytic flora, which went on to dominate terrestrial habitats during the Carboniferous. This new vegetation type included early seed plants such as Calamopityales and Lyginopteridales. The development of seeds as part of their reproductive and dispersal strategies freed the plants from requiring moisture for gametophyte fertilization, resulting in far fewer constraints on the spatial distribution of vegetation (Algeo and Scheckler, 1998). Seeds allowed the Paleophytic vegetation to spread into a much wider range of terrestrial habitats during the Famennian and Mississippian, causing a significant increase in the total biomass of plants. Again, these innovations did not apparently alter long-term $\delta^{238}U$ trends.

4.6. Emsian-Eifelian oxygenation event

Previous studies report a major rise in atmospheric oxygen levels sometime during the late Silurian to Devonian (a potential time span of ~60 Myr) and interpreted this rise as the result of terrestrial floral expansion and a resultant increase in organic carbon burial (Algeo and Scheckler, 1998; Algeo and Ingall, 2007; Dahl et al., 2010; Sperling et al., 2015, 2021; Lenton et al., 2016; Wallace et al., 2017; Lu et al., 2018). Some of these previous studies specifically argue that the atmospheric O_2 rise was the result of the appearance of refractory organic matter or lignin. Lignin occurs as early as the Early Devonian (progymnosperms) and the Eifelian, but these did not become large plants until the Givetian and were not widespread until the Frasnian and especially the Famennian (Algeo and Scheckler, 1998). Results from this study constrain the timing of the most significant phase of the oxygenation event to the EEB (~395 Ma). The timing of this oxygenation rise is consistent with the inference that late Silurian through Early Devonian plant diversification and, in particular, the shift from smaller Early Eophytic to larger Late Eophytic taxa along with their spread into a wider array of environments triggered increased photosynthesis, organic carbon burial, and atmospheric O_2 buildup. This pO_2 increase then tipped the oceans into a more oxygenated state characteristic of the post-Middle Devonian and beyond.

A key interpretation of the present study is that the Emsian-Eifelian oxygenation event was related to the evolution and diversification of land plants, and specifically the appearance of the Late Eophytic flora. Thus, these paleobotanical developments may have been the primary driver of rising atmospheric O_2 levels rather than the spread of true forests, increases in tree height, lignin content, root depth, and the advent of seeds in the Late Devonian. However, the Late Eophytic flora, despite consisting of larger plants with deeper roots, was constrained to moist riparian and wetland areas in lowland coastal regions due to their pteridophytic (spore-bearing) reproductive mechanisms. Thus, it may be inferred that these habitats supported plant communities whose biomass and organic matter burial rates were sufficient to cause significant oxygenation of the Earth's atmosphere and oceans. The resultant increase in seawater oxygenation was likely aided by cooler Middle Devonian SSTs (Joachimski et al., 2009).

There is a positive ~2‰ $\delta^{13}C$ shift across the EEB that may signal part of the interpreted plant carbon burial signal; part may also have been removed along the unconformity. We acknowledge that there are other positive $\delta^{13}C$ shifts of similar magnitude in the record, but none of these shifts are associated with a similar magnitude of $\delta^{238}U$ shift. This does not invalidate our argument of plant carbon burial driving the EEB oxygenation event, it simply means that coupling of the C cycle and ocean oxygenation is more complex than an assumed and overly simplistic 1:1 response. Potential complexities may include that the EEB marks oxygenation of the ocean-surface layer which would have limited U sequestration in shelf deposits (where most organic matter is buried) and thus limited impacts on overall organic carbon burial rates. Other non-global explanations may include changes in ocean circulation or ocean-basin configuration.

Additional continuous high-resolution global-ocean redox data for the early Paleozoic are needed to ascertain whether reducing conditions persisted continuously from the Neoproterozoic through the Early Devonian. A recent Fe-speciation record spanning the early and middle Paleozoic in the Canadian Richardson Trough, along with compiled data from other deeper ocean basins, suggests predominantly anoxic bottom waters through the entire early to middle Paleozoic (Sperling et al., 2021). In particular, that record suggests a shift from predominantly ferruginous anoxic conditions during the early Paleozoic to locally euxinia conditions in the Early Devonian (Pragian). However, this shift may represent a localized phenomenon in a Devonian deep-water basin (i.e., Richardson Trough) because of increased primary productivity/export production (linked to plant-weathering feedbacks), despite higher pO_2 and more oxygenated surface oceans. The apparent offset in timing between the Sperling et al. Pragian shift and this study's Emsian-Eifelian shift may be due to the difference between graptolite- vs conodont-based age models and the relatively poor stage-level age control and relative stratigraphic condensation in that particular interval of the Sperling et al. data.

Our new results lend support to the interpretation that the EEB event was a significant oxygenation state change marking a transition between the reducing conditions of the Proterozoic-early Paleozoic oceans and the more oxygenated oceans of the middle-late Paleozoic to Recent oceans. Alternatively, Proterozoic to middle Paleozoic global oceans may have been characterized by alternating ~10^7-Myr intervals of more reducing and more oxic conditions (Wei et al., 2021), implying that the EEB oxygenation event represents the final shift to fully oxygenated oceans. In either scenario, the Emsian-Eifelian oxygenation event was a major turning point in Earth's redox history and paved the way for the broad diversity of large, mobile animals that have dominated both marine and terrestrial environments over the past 400 Myr.

5. Conclusions

1) Detailed stratigraphy, U-C-O isotopes, and elemental concentrations in biostratigraphically well-dated marine carbonates across Laurentia (Nevada and Illinois) were used to investigate high-resolution seawater redox trends spanning ~70 Myr from the late Silurian to Early Mississippian.
2) Stratigraphic and geochemical trends from the two widely separated (>2800 km) Laurentian locations indicate that most of the Nevada $\delta^{238}U$ records represents a near-primary global marine signal.
3) First-order $\delta^{238}U$ trends are consistent with predominantly reducing oceans from the late Silurian (Pridoli) through the Early Devonian (~20 Myr) with an oxic excursion near the Lochkovian-Pragian boundary. A large oxygen rise occurred in <4 Myr near the Early-Middle Devonian boundary at ~395 Ma (Emsian-Eifelian boundary), and more oxygenated seawater conditions continued for the next 30(+) Myr through the Middle-Late Devonian and Early Mississippian.
4) Superimposed on the more oxic Middle-Late Devonian and Early Mississippian seawater conditions are seven high-frequency (Myr-scale) anoxic events which correlate with known global biotic crises-extinctions, positive $\delta^{13}C$ excursions, and abundant anoxic facies deposition.
5) This new ~70 Myr-long, high-resolution seawater redox record suggests that the prominent Emsian-Eifelian oxygenation event represented a major state change between strongly reducing mid-late Silurian and Early Devonian oceans and more oxygenated Middle-Late Devonian and Early Mississippian oceans. In fact, the Emsian-Eifelian oxygenation event may mark a major biogeochemical transformation in Earth history between prolonged reducing Proterozoic-early Paleozoic oceans and well-oxygenated oceans of the middle-late Paleozoic through Recent.
6) The timing of the oxygenation event is consistent with the interpretation that pO_2 build-up was the result of the increased biomass/photosynthesis and burial of late Silurian through earliest Middle Devonian plants rather than of paleobotanical innovations such as arborescence, increased lignin, and seed habit, which developed later in the Devonian. This implies that early land plants characterized by shallower roots and geographically constrained to moist riparian and lowland coastal regions had sufficient biomass to drive long-term oxygenation of the ocean-atmosphere system, paving the way for the evolution of large, mobile animals that have dominated marine and terrestrial environments since the middle Paleozoic.
7) Our new seawater redox curve provides an important baseline to further investigate links between seawater redox trends and a wide range of Earth system processes, analogous to the wealth of information provided by secular O-C-Sr isotope curves.

CRediT authorship contribution statement

Conceptualization – ME, GG, SR, TA, JM.
Methodology – ME, GG, SR, TA, JM, MS, TG, PC, CC, BCM.
Supervision – ME, GG, SR, JM.
Writing, original – ME, GG.
Writing, review – ME, GG, SR, TA, JM, PC, CC, BCM.
Fund acquisition – ME, GG, SR, TA, JM, BCM.
Project administration – ME.

Declaration of competing interest

The authors declare that they have no known competing financial interests or personal relationships that could have appeared to influence the work reported in this paper.

Acknowledgements

Many thanks for the invaluable lab and field assistance from Chadlin Ostrander, Jed Day, Zunli Lu, Ruliang He, Patrick Kelly, Zoe Wiesel, Elizabeth Driscoll, Kate Meyers, Sam Patzkowsky, Monica Charles, and Kobie Boslough. The research was funded by National Science Foundation grant EA-1733991 (ME, SR, TA, JM, GG), NASA (GJG), and EARTHGREEN project ANR-20-CE01-0002-01 (BCM).

Appendix A. Supplementary material

Supplementary material related to this article can be found online at https://doi.org/10.1016/j.epsl.2022.117410.

References

Algeo, T.J., Scheckler, S.E., 1998. Terrestrial-marine teleconnections in the Devonian: links between the evolution of land plants, weathering processes, and marine anoxic events. Philos. Trans. R. Soc. Lond. B 353, 113–130.

Algeo, T.J., Ingall, E., 2007. Sedimentary C_{org}:P ratios, paleocean ventilation, and Phanerozoic atmospheric pO_2. Palaeogeogr. Palaeoclimatol. Palaeoecol. 256, 130–155.

Andersen, M.B., Stirling, C.H., Weyer, S., 2017. Uranium isotope fractionation. Rev. Mineral. Geochem. 82, 799–850.

Becker, R.T., Königshof, P., Brett, C.E., 2016. Devonian Climate, Sea Level and Evolutionary Events: an Introduction. Devonian Climate, Sea Level and Evolutionary Events, vol. 423. Geol. Soc. London Spec. Publ., pp. 1–10.

Becker, R.T., Marshall, J.E.A., Da Silva, A.C., Agterberg, F.P., Gradstein, F.M., Ogg, J.G., 2020. The Devonian period. In: Geologic Time Scale 2020. Elsevier, pp. 733–810.

Berner, R.A., 1998. The carbon cycle and carbon dioxide over Phanerozoic time: the role of land plants. Philos. Trans. R. Soc. Lond. B 353, 75–82.

Berner, R.A., 2006. GEOCARBSULF: a combined model for Phanerozoic atmospheric O_2 and CO_2. Geochim. Cosmochim. Acta 70, 5653–5664.

Bowman, C.N., Young, S.A., Kaljo, D., Eriksson, M.E., Them, T.R., Hints, O., Martma, T., Owens, J.D., 2019. Linking the progressive expansion of reducing conditions to a stepwise mass extinction event in the late Silurian oceans. Geology 47, 968–972.

Bowman, C.N., Lindskog, A., Kozik, N.P., Richbourg, C.G., Owens, J.D., Young, S.A., 2020. Integrated sedimentary, biotic, and paleoredox dynamics from multiple localities in southern Laurentia during the late Silurian (Ludfordian) extinction event. Palaeogeogr. Palaeoclimatol. Palaeoecol. 553, 109799.

Brennecka, G.A., Herrmann, A.D., Algeo, T.J., Anbar, A.D., 2011. Rapid expansion of oceanic anoxia immediately before the end-Permian mass extinction. Proc. Natl. Acad. Sci. USA 108, 17631–17634.

Bruggmann, S., Gilleaudeau, G.J., Romaniello, S.J., Severmann, S., Canfield, D.E., Anbar, A.D., Scholz, F., Frei, R., 2022. Uranium isotope cycling on the highly productive Peruvian margin. Chem. Geol. 590, 120705.

Buggisch, W., Joachimski, M.M., 2006. Carbon isotope stratigraphy of the Devonian of central and southern Europe. Palaeogeogr. Palaeoclimatol. Palaeoecol. 240, 68–88.

Calner, M., 2008. Silurian global events–at the tipping point of climate change. In: Mass Extinction. Springer, Berlin, pp. 21–57.

Capel, E., Cleal, C.J., Gerrienne, P., Servais, T., Cascales-Miñana, B., 2021. A factor analysis approach to modelling the early diversification of terrestrial vegetation. Palaeogeogr. Palaeoclimatol. Palaeoecol. 566, 110170.

Cascales-Miñana, B., 2016. Apparent changes in the Ordovician–Mississippian plant diversity. Rev. Palaeobot. Palynol. 227, 19–27.

Cascales-Miñana, B., Diez, J.B., Cleal, C.J., 2013. What is the best way to measure extinction? A reflection from the palaeobotanical record. Earth-Sci. Rev. 124, 126–147.

Chen, X., Romaniello, S.J., Herrmann, A.D., Hardisty, D., Gill, B.C., Anbar, A.D., 2018. Diagenetic effects on uranium isotope fractionation in carbonate sediments from the Bahamas. Geochim. Cosmochim. Acta 237, 294–311.

Chen, X., Tissot, F.L.H., Jansen, M.F., Bekker, A., Liu, C.X., Nie, N.X., Halverson, G.P., Veizer, J., Dauphas, N., 2021a. The uranium isotopic record of shales and carbonates through geologic time. Geochim. Cosmochim. Acta 300, 164–191.

Chen, B., Ma, X., Mills, B.J., Qie, W., Joachimski, M.M., Shen, S., Wang, C., Xu, H., Wang, X., 2021b. Devonian paleoclimate and its drivers: a reassessment based on a new conodont $\delta^{18}O$ record from South China. Earth-Sci. Rev. 222, 103814.

Cheng, K., Elrick, M., Romaniello, S.J., 2020. Early Mississippian ocean anoxia triggered organic carbon burial and late Paleozoic cooling: evidence from uranium isotopes recorded in marine limestone. Geology 48, 363–367.

Chlupáč, I., Kukal, Z., 1986. Reflection of possible global Devonian events in the Barrandian area, CSSR. In: Global Bio-Events. Springer, Berlin, pp. 169–179.

Clarkson, M.O., Stirling, C.H., Jenkyns, H.C., Dickson, A.J., Porcelli, D., Moy, C.M., von Strandmann, P.A.P., Cooke, I.R., Lenton, T.M., 2018. Uranium isotope evidence for two episodes of deoxygenation during Oceanic Anoxic Event 2. Proc. Natl. Acad. Sci. USA 115, 2918–2923.

Clarkson, M.O., Müsing, K., Andersen, M.B., Vance, D., 2020. Examining pelagic carbonate-rich sediments as an archive for authigenic uranium and molybdenum isotopes using reductive cleaning and leaching experiments. Chem. Geol. 539, 119412.

Cleal, C.J., Cascales-Miñana, B., 2021. Evolutionary floras – revealing large-scale patterns in Palaeozoic vegetation history. J Palaeosci. 70, 31–42.

Cole, D.B., Planavsky, N.J., Longley, M., Böning, P., Wilkes, D., Wang, X., Swanner, E.D., Wittkop, C., Loydell, D.K., Busigny, V., Knudsen, A.C., 2020. Uranium isotope fractionation in non-sulfidic anoxic settings and the global uranium isotope mass balance. Glob. Biogeochem. Cycles 34, e2020GB006649.

Dahl, T.W., Hammarlund, E.U., Anbar, A.D., Bond, D.P., Gill, B.C., Gordon, G.W., Knoll, A.H., Nielsen, A.T., Schovsbo, N.H., Canfield, D.E., 2010. Devonian rise in atmospheric oxygen correlated to the radiations of terrestrial plants and large predatory fish. Proc. Natl. Acad. Sci. USA 107, 17911–17915.

Dahl, T.W., Boyle, R.A., Canfield, D.E., Connelly, J.N., Gill, B.C., Lenton, T.M., Bizzarro, M., 2014. Uranium isotopes distinguish two geochemically distinct stages during the late Cambrian SPICE event. Earth Planet. Sci. Lett. 401, 313–326.

D'Antonio, M., Ibarra, D.E., Boyce, C.K., 2020. Land plant evolution decreased, rather than increased, weathering rates. Geology 48, 29–33.

del Rey, Á., Havsteen, J.C., Bizzarro, M., Dahl, T.W., 2020. Untangling the diagenetic history of uranium isotopes in marine carbonates: a case study tracing the $\delta^{238}U$ composition of late Silurian oceans using calcitic brachiopod shells. Geochim. Cosmochim. Acta 287, 93–110.

del Rey, Á., 2021. Reconstructing global ocean oxygenation during critical mid Paleozoic events and how global changes in the redox landscape of the oceans relate to marine animal life. Ph.D. Dissertation. University of Copenhagen, Denmark. 169 pp.

Edwards, D., Fanning, U., Richardson, J.B., 1986. Stomata and sterome in early land plants. Nature 23, 438–440.

Elrick, M., Polyak, V., Algeo, T.J., Romaniello, S., Asmerom, Y., Herrmann, A.D., Anbar, A.D., Zhao, L., Chen, Z., 2017. Global-ocean redox variation during the middle-late Permian through Early Triassic based on uranium isotope and Th/U trends of marine carbonates. Geology 45, 163–166.

Gilleaudeau, G.J., Romaniello, S.J., Luo, G., Kaufman, A.J., Zhang, F., Klaebe, R.M., Kah, L.C., Azmy, K., Bartley, J.K., Zheng, W., Knoll, A.H., 2019. Uranium isotope evidence for limited euxinia in mid-Proterozoic oceans. Earth Planet. Sci. Lett. 521, 150–157.

Gilleaudeau, G.J., Algeo, T.J., Lyons, T.W., Bates, S., Anbar, A.D., 2021. Novel watermass reconstruction in the Early Mississippian Appalachian Seaway based on integrated proxy records of redox and salinity. Earth Planet. Sci. Lett. 558, 116746.

He, R., Elrick, M., Day, J.E., Lu, W., Lu, Z., 2021. Devonian upper ocean redox trends across Laurussia: testing potential influence of marine carbonate facies on bulk rock I/Ca signal. In: AGU Fall Meeting 2021.

Herrmann, A.D., Gordon, G., Anbar, A.D., 2018. Uranium isotope variations in a dolomitized Jurassic carbonate platform (Tithonian; Franconian Alb, Southern Germany). Chem. Geol. 497, 41–53.

Hetherington, S., Bridson, S.L., Jones, A.L., Hass, H., Kerp, H., Dolan, L., 2021. An evidence-based 3D reconstruction of Asteroxylon mackiei the most complex plant preserved from the Rhynie chert. eLife 10, e69447.

Joachimski, M.M., Breisig, S., Buggisch, W., Talent, J.A., Mawson, R., Gereke, M., Morrow, J.R., Day, J., Weddige, K., 2009. Devonian climate and reef evolution: insights from oxygen isotopes in apatite. Earth Planet. Sci. Lett. 284, 599–609.

Johnson, J.G., Klapper, G., Sandberg, C.A., 1985. Devonian eustatic fluctuations in Euramerica. Geol. Soc. Am. Bull. 96, 567–587.

Johnson, J.G., Klapper, G., Elrick, M., 1996. Devonian transgressive-regressive cycles and biostratigraphy, northern Antelope Range, Nevada; Establishment of reference horizons for global cycles. Palaios 11, 3–14.

Jost, A.B., Bachan, A., van de Schootbrugge, B., Lau, K.V., Weaver, K.L., Maher, K., Payne, J.L., 2017. Uranium isotope evidence for an expansion of marine anoxia during the end-Triassic extinction. Geochem. Geophys. Geosyst. 18, 3093–3108.

Kah, L.C., Lyons, T.W., Frank, T.D., 2004. Low marine sulphate and protracted oxygenation of the Proterozoic biosphere. Nature 431, 834–838.

Kenrick, P., Wellman, C.H., Schneider, H., Edgecombe, G.D., 2012. A timeline for terrestrialization: consequences for the carbon cycle in the Palaeozoic. Philos. Trans. - R. Soc., Biol. Sci. 367 (1588), 519–536.

Kolata, D.R., Nelson, W.J., 1990. Tectonic history of the Illinois basin: Chapter 18: part I. In: Illinois Basin: Evolution.

Krause, A.J., Mills, B.J., Zhang, S., Planavsky, N.J., Lenton, T.M., Poulton, S.W., 2018. Stepwise oxygenation of the Paleozoic atmosphere. Nat. Commun. 9, 1–10.

Laakso, T.A., Schrag, D.P., 2014. Regulation of atmospheric oxygen during the Proterozoic. Earth Planet. Sci. Lett. 388, 81–91.

Lau, K.V., Maher, K., Altiner, D., Kelley, B.M., Kump, L.R., Lehrmann, D.J., Silva-Tamayo, J.C., Weaver, K.L., Yu, M., Payne, J.L., 2016. Marine anoxia and delayed Earth system recovery after the end-Permian extinction. Proc. Natl. Acad. Sci. USA 113, 2360–2365.

Lenton, T.M., Dahl, T.W., Daines, S.J., Mills, B.J., Ozaki, K., Saltzman, M.R., Porada, P., 2016. Earliest land plants created modern levels of atmospheric oxygen. Proc. Natl. Acad. Sci. USA 113, 9704–9709.

Livermore, B.D., Dahl, T.W., Bizzarro, M., Connelly, J.N., 2020. Uranium isotope compositions of biogenic carbonates–implications for U uptake in shells and the application of the paleo-ocean oxygenation proxy. Geochim. Cosmochim. Acta 287, 50–64.

Lu, W., Ridgwell, A., Thomas, E., Hardisty, D.S., Luo, G., Algeo, T.J., Saltzman, M.R., Gill, B.C., Shen, Y., Ling, H.-F.J.S., et al., 2018. Late inception of a resiliently oxygenated upper ocean. Science 361, 174–177.

McLennan, S.M., 2001. Relationships between the trace element composition of sedimentary rocks and upper continental crust. Geochem. Geophys. Geosyst. 2. https://doi.org/10.1029/2000gc000109.

Melchin, M.J., Sadler, P.M., Cramer, B.D., 2020. The Silurian period. In: Geologic Time Scale 2020. Elsevier, pp. 695–732.

Meyer-Berthaud, B., Soria, A., Decombeix, A.L., 2010. The land plant cover in the Devonian: a reassessment of the evolution of the tree habit. In: Vecoli, M., Clément, G., Meyer-Berthaud, B. (Eds.), The Terrestrialization Process: Modelling Complex Interactions at the Biosphere–Geosphere Interface. In: Geol. Soc. Lond. Spec. Publ., vol. 339, pp. 59–70.

Planavsky, N.J., Reinhard, C.T., Wang, X., Thomson, D., McGoldrick, P., Rainbird, R.H., Johnson, T., Fischer, W.W., Lyons, T.W., 2014. Low mid-Proterozoic atmospheric oxygen levels and the delayed rise of animals. Science 346, 635–638.

Romaniello, S.J., Herrmann, A.D., Anbar, A.D., 2013. Uranium concentrations and $^{238}U/^{235}U$ isotope ratios in modern carbonates from the Bahamas: assessing a novel paleoredox proxy. Chem. Geol. 362, 305–316.

Saltzman, M.R., Thomas, E., Gradstein, F.M., 2012. Carbon isotope stratigraphy. In: The Geologic Time Scale 2012, vol. 1, pp. 207–232.

Schneider, P.J., 1990. An algorithm for automatically fitting digitized curves. In: Graphics Gems, vol. 1, pp. 612–626.

Scott, A.C., Glasspool, I.J., 2006. The diversification of Paleozoic fire systems and fluctuations in atmospheric oxygen concentration. Proc. Natl. Acad. Sci. USA 103, 10861–10865.

Sepkoski Jr., J.J., 1984. A kinetic model of Phanerozoic taxonomic diversity. III. Post Paleozoic families and mass extinctions. Paleobiology 10, 246–267.

Servais, T., Cascales-Miñana, B., Cleal, C.J., Gerrienne, P., Harper, D.A., Neumann, M., 2019. Revisiting the Great Ordovician Diversification of land plants: recent data and perspectives. Palaeogeogr. Palaeoclimatol. Palaeoecol. 534, 109280.

Smith, A.B., McGowan, A.J., 2007. The shape of the Phanerozoic marine palaeodiversity curve: how much can be predicted from the sedimentary rock record of western Europe? Palaeontol. 50, 765–774.

Song, H.Y., Song, H.J., Algeo, T.J., Tong, J., Romaniello, S.J., Zhu, Y., Chu, D., Gong, Y., Anbar, A.D., 2017. Uranium and carbon isotopes document global-ocean redox-productivity relationships linked to cooling during the Frasnian-Famennian mass extinction. Geology 45, 887–890.

Song, Y., Gilleaudeau, G.J., Algeo, T.J., Over, D.J., Lyons, T.W., Anbar, A.D., Xie, S., 2021. Biomarker evidence of algal-microbial community changes linked to redox and salinity variation, Upper Devonian Chattanooga Shale (Tennessee, USA). GSA Bull. 133 (1–2), 409–424.

Sperling, E.A., Wolock, C.J., Morgan, A.S., Gill, B.C., Kunzmann, M., Halverson, G.P., Macdonald, F.A., Knoll, A.H., Johnston, D.T., 2015. Statistical analysis of iron geochemical data suggests limited late Proterozoic oxygenation. Nature 523, 451–454.

Sperling, E.A., Melchin, M.J., Fraser, T., Stockey, R.G., Farrell, U.C., Bhajan, L., Brunoir, T.N., Cole, D.B., Gill, B.C., Lenz, A., Loydell, D.K., 2021. A long-term record of early to mid-Paleozoic marine redox change. Sci. Adv. 7, eabf4382.

Spotl, C., Vennemann, T.W., 2003. Continuous-flow isotope mass spectrometric analysis of carbonate minerals. Rapid Commun. Mass Spectrom. 17, 1004–1006.

Stirling, C.H., Andersen, M.B., Warthmann, R., Halliday, A.N., 2015. Isotope fractionation of ^{238}U and ^{235}U during biologically-mediated uranium reduction. Geochim. Cosmochim. Acta 163, 200–218.

Stylo, M., Neubert, N., Wang, Y., Monga, N., Romaniello, S.J., Weyer, S., Bernier-Latmani, R., 2015. Uranium isotopes fingerprint biotic reduction. Proc. Natl. Acad. Sci. USA 112, 5619–5624.

Taylor, S.R., McLennan, S.M., 1985. The Continental Crust: Its Composition and Evolution. Blackwell, Malden, MA.

Tissot, F.L.H., Dauphas, N., 2015. Uranium isotopic compositions of the crust and ocean: age corrections, U budget and global extent of modern anoxia. Geochim. Cosmochim. Acta 167, 113–143.

Tissot, F.L.H., Chen, C., Go, B.M., Naziemiec, M., Healy, G., Bekker, A., Swart, P.K., Dauphas, N., 2018. Controls of eustasy and diagenesis on the $^{238}U/^{235}U$ of carbonates and evolution of the seawater ($^{234}U/^{238}U$) during the last 1.4 Myr. Geochim. Cosmochim. Acta 242, 233–265.

van Geldern, R., Joachimski, M.M., Day, J., Jansen, U., Alvarez, F., Yolkin, E.A., Ma, X.P., 2006. Carbon, oxygen and strontium isotope records of Devonian brachiopod shell calcite. Palaeogeogr. Palaeoclimatol. Palaeoecol. 240, 47–67.

Wallace, M.W., Shuster, A., Greig, A., Planavsky, N.J., Reed, C.P., 2017. Oxygenation history of the Neoproterozoic to early Phanerozoic and the rise of land plants. Earth Planet. Sci. Lett. 466, 12–19.

Wang, X., Planavsky, N.J., Reinhard, C.T., Hein, J.R., Johnson, T.M., 2016. A Cenozoic seawater redox record derived from $^{238}U/^{235}U$ in ferromanganese crusts. Am. J. Sci. 316, 64–83.

Wei, G.Y., Planavsky, N.J., He, T., Zhang, F., Stockey, R., Cole, D.B., Lin, Y.B., Ling, H.F., 2021. Global marine redox evolution from the late Neoproterozoic to the early Paleozoic constrained by the integration of Mo and U isotope records. Earth-Sci. Rev. 214, 103506.

Wellman, C.H., Steemans, P., Vecoli, M., 2013. Palaeophytogeography of Ordovician-Silurian land plants. In: Harper, D.A.T., Servais, T. (Eds.), Early Palaeozoic Biogeography and Palaeogeography. Geological Society Memoirs, London, pp. 461–476.

Weyer, S., Anbar, A.D., Gerdes, A., Gordon, G.W., Algeo, T.J., Boyle, E.A., 2008. Natural fractionation of $\delta^{238}U$. Geochim. Cosmochim. Acta 72, 345–359.

White, D.A., Elrick, M., Romaniello, S., Zhang, F., 2018. Global seawater redox trends during the Late Devonian mass extinction detected using U isotopes of marine limestones. Earth Planet. Sci. Lett. 503, 68–77.

Young, S.A., Kleinberg, A., Owens, J.D., 2019. Geochemical evidence for expansion of marine euxinia during an early Silurian (Llandovery–Wenlock boundary) mass extinction. Earth Planet. Sci. Lett. 513, 187–196.

Zhang, S., Wang, X., Wang, H., Bjerrum, C.J., Hammarlund, E.U., Mafalda Costa, M., Connelly, J.N., Zhang, B., Su, J., Canfield, D.E., 2016. Sufficient oxygen for animal respiration 1,400 million years ago. Proc. Natl. Acad. Sci. USA 113, 1731–1736.

Zhang, F., Algeo, T.J., Romaniello, S.J., Cui, Y., Zhao, L., Chen, Z.Q., Anbar, A.D., 2018. Congruent Permian-Triassic $\delta^{238}U$ records at Panthalassic and Tethyan sites: confirmation of global-oceanic anoxia and validation of the U-isotope paleoredox proxy. Geology 46, 327–330.